# Modeling Breaking Waves and Wave-induced Currents with Fully Nonlinear Boussinesq Equations

K.Z. FANG[1,2*], Z.B. LIU[1,2]
[1]the State Key Laboratory of Coastal and Offshore Engineering
Dalian University of Technology
Linggong Road 2, 116024 Dalian
[2]Key Laboratory of Water-Sediment Sciences and Water Disaster prevention of Hunan Province
Changsha University of Technology
Chiling Road 45, 410004 Changsha
CHINA
*kfang@dlut.edu.cn

*Abstract:* A Boussinesq-type wave model is developed to numerically investigate the breaking waves and wave-induced currents. All the nonlinear terms are retained in the governing equations to keep fully nonlinearity characteristics and it hence more suitable to describe breaking waves with strong nonlinearity in the nearshore region. The Boussinesq equations are firstly extended to incorporate wave breaking, moving shoreline and bottom friction, and then solved numerically using finite difference method. Using well documented experimental data as a reference, numerical experiments are conducted to investigate the effect of tunable parameter values on the computed results. The developed model is used to simulate breaking waves and wave-induced currents over complex bathymetries and the numerical results are compared against the measurements.

*Key-Words:* - Breaking waves, Wave-induced currents, Boussinesq-type wave model, Numerical simulation.

## 1 Introduction

Originating from the pioneering contributions made by Boussinesq [1], Korteweg and de Vries [2], and Peregrine [3], recent research efforts have provided a solid theoretical background for a new generation of the so-called Boussinesq-type wave equations. With the increase of the computation ability, numerical models based on this kind of equations have proven to adequately describe most of the water wave phenomena taking place in the nearshore zone, see recent reviews by Kirby [4].

The development of Boussinesq-type equations usually involves two parameters, namely $\mu$=(ratio of typical water depth to wave length) and $\varepsilon$ (ratio of typical wave amplitude to water depth). $\mu$ denotes the dispersion and the limit $\mu$=0 represents the non-dispersive limit. $\varepsilon$ characterizes the nonlinearity and the limit $\varepsilon$=0 represents the linear limit. These two parameters are usually assumed small ($\leq$1) in deriving Boussinesq-type equations, referring to weakly dispersive and weakly nonlinear regimes.

In the recent past, great studies have been made to improve the linear properties of Boussinesq-type equations. Since the weak dispersion ($\mu\leq$1) is the most critical limitation for many applications, most of work has focused on extending models' applicability range to deep water. Abundant research results have been published and the applicability range of the equations has been greatly improved (e.g., Madsen et al. [5]; Madsen and Sørensen[6]; Nwogu[7]; Madsen and Schäffer [8]; Madsen et al. [9]; Gobbi and Kirby [10]; Zou and Fang [11]). The linear shoaling property could not be ignored considering the applicable range of water depth is enlarged for many new forms of Boussinesq-type equations. In many improved models (Madsen and Sørensen [6]; Zou [12]; Gobbi and Kirby [10]; Zou and Fang [11]), attention has also been given to the shoaling property of equations.

Despite their improved linear properties, the extended Boussinesq equations are still restricted to situations with weak nonlinearity (i.e., $\varepsilon\leq$1). In many practical cases, however, the effects of nonlinearity are too large to be treated as a weak perturbation to a primarily linear problem. For example, $\varepsilon$ approaches 1 for the wave motion near the breaking point(due to the effect of shoaling) and can't be assumed a small value anymore. And thus extensions are required in order to obtain a computational tool which is locally valid in the

vicinity of a steep, almost breaking or breaking wave crest. Wei et al. [13] relaxed the limitations of weak nonlinearity ($\varepsilon \leq 1$) and retained all the nonlinear terms in the equations, thus creating a fully nonlinear Boussinesq-type model at the order of $O(\mu^2)$. Lately, Gobbi and Kirby [10], Zou and Fang [11] derived fourth-order Boussinesq-type equations with fully nonlinear characteristics. For nonbreaking waves with strong nonlinearity, these studies have shown that fully nonlinear models could present better numerical results than weakly nonlinear models. This conclusion is also valid for a solitary wave shoaling up to the breaking point [13], and for breaking waves [14].

Though Boussinesq-type models have already been brought into the family of operational coastal wave prediction models, the applications of such models with fully nonlinearity in surf zone is quite limited yet, except FUNWAVE2D model [15]. This model, based on the fully nonlinear version of Boussinesq equations presented by Wei et al. [13], has been extensively tested for their applicability in modeling nearshore waves and currents [13]-[19]. Wave breaking, moving shoreline and other mechanisms are common physical phenomena in surf and swash zone but approximately treated in Boussinesq-type models, and thus many tunable parameters are introduced. Previous studies also underline the scarcity of the detailed investigation of parameter values on the numerical results. Additionally the applicability of Boussinesq-type equations, formulated in other forms, in surf zone has received considerably less attention yet.

The requirement for further investigation are further amplified for 2D breaking waves as they always induce relatively long scale wave motions, such as mean currents, which have been long recognized to play a key role in coastal ecology and morphology. Usually phase-averaged type models are adopted to simulate mean currents, the effect of short waves is considered by computing the radiation stress for a separate run of a wave-averaged model, where the effect of nonlinearities such as the interaction between waves, waves and currents, wave asymmetry and etc. can only be included in an approximate manner. While the Boussinesq-type models have the capabilities of modeling nonlinear short wave motions and fully coupled wave-current interaction [16][17]. All these advantages enable the Boussinesq approach, especially those with fully nonlinearity characteristics, a promising and an alternative tool for the study of low-frequency motions, superior to the phase-averaged type models.

The present paper develops a 2D wave breaking model, based on a set of fully nonlinear Boussinesq-type equations. In section 2, the mathematical model is described. In section 3, the numerical experiments are conducted to investigate the effect of parameters on the computed results. And the validated model is used to simulate nonlinear evolution of breaking waves and wave-induced currents over plane and barred beaches. The final conclusions are drawn in section 4.

# 2 Mathematical Model

## 2.1 Governing Equations

The second order Boussinesq equations derived by Zou [20] are expressed in terms of free surface elevation $\eta$ and depth-averaged velocity $\boldsymbol{u}$ as

$$\eta_t + \nabla \cdot (d\boldsymbol{u}) = 0 \tag{1}$$

$$\begin{aligned} \boldsymbol{u}_t &+ (\boldsymbol{u}\cdot\nabla)\boldsymbol{u} + g\nabla\eta + \boldsymbol{G} = h\nabla[\nabla\cdot(h\boldsymbol{u})_t]/2 \\ &- h^2\nabla(\nabla\cdot\boldsymbol{u}_t)/6 + B_1 h^2\nabla[\nabla\cdot(\boldsymbol{u}_t + g\nabla\eta)] \\ &+ B_2\nabla[\nabla\cdot(h^2\boldsymbol{u}_t + gh^2\nabla\eta)] + \boldsymbol{R} \end{aligned} \tag{2}$$

$$\begin{aligned} \boldsymbol{G} &= \nabla\{h^2[(\nabla\cdot\boldsymbol{u})^2 - \boldsymbol{u}\cdot\nabla^2\boldsymbol{u} - B_3\nabla^2(\boldsymbol{u}\cdot\boldsymbol{u})/10]\}/3 \\ &- \nabla\eta h\nabla\cdot\boldsymbol{u}_t \end{aligned}$$

where the subscript $t$ denotes the partial derivative with respect to time, $\nabla = (\partial_x, \partial_y)$ is the two dimensional gradient operator, $h$ is the still water depth and $d=h+\eta$ is local water depth, $g$ the gravity acceleration. $B_1$ and $B_2$ are set to be 29/885, 2/59 respectively after matching equations' dispersion to a Padé[2,2] approximation of the exact linear dispersion and optimizing the shoaling property in medium water depth limit. While $B_3$=5.3 is chosen to get optimum nonlinear property within the applicable range of the equations. $\boldsymbol{R}=\boldsymbol{R}_b+\boldsymbol{R}_f+\boldsymbol{R}_s$ is the extended term for wave breaking, bottom friction and subgrid mixing and will be detailed in the next subsection. However in the above equations, nonlinear terms are only retained up to the order of $O(\varepsilon\mu^2)$ under the assumption of $\varepsilon \leq 1$ thus the equations only possess weak nonlinearity. After relaxing this limitations and retaining all the nonlinear terms, the nonlinear term $\boldsymbol{G}$ has the form of

$$\begin{aligned} \boldsymbol{G} &= \nabla\{d^2[(\nabla\cdot\boldsymbol{u})^2 - \boldsymbol{u}\cdot\nabla^2\boldsymbol{u} - B_3\nabla^2(\boldsymbol{u}\cdot\boldsymbol{u})/10]\}/3 \\ &+ \nabla\eta d[(\nabla\cdot\boldsymbol{u})^2 - \boldsymbol{u}\cdot\nabla^2\boldsymbol{u}]/3 - \nabla\eta d\nabla\cdot\boldsymbol{u}_t \\ &- \eta(2h+\eta)\nabla(\nabla\cdot\boldsymbol{u}_t)/3 \end{aligned} \tag{4}$$

Hereafter,(1)-(3) are named weakly nonlinear model while, equations (1)-(2) with $\boldsymbol{G}$ defined by (4) are named fully nonlinear model.

## 2.2 Extend Governing Equations to Surf and Swash Zone

Energy dissipation due to wave breaking is treated by introducing an eddy viscosity term($\boldsymbol{R}_b$) into the momentum equations, with the viscosity strongly localized on the front face of the breaking waves (Kennedy et al. [14]; Chen et al. [16] )

$$\boldsymbol{R}_b = (h+\eta)^{-1}\nabla\cdot[\nu(h+\eta)(\nabla\boldsymbol{u}+(\nabla\boldsymbol{u})^T)] \quad (5)$$

where the eddy viscosity is defined as $\nu=BC_{br}^2\left|d\boldsymbol{u}\right|$, with $C_{br}$ =1.2 being the default breaking strength coefficient. The parameter $B$ controls the occurrence of the wave dissipation and is given by

$$B=\begin{cases}1, & \eta_t \geq 2\eta_t^* \\ \eta_t/\eta_t^*, & \eta_t^* < \eta_t \leq 2\eta_t^* \\ 0, & \eta_t \leq \eta_t^*\end{cases} \quad (6)$$

The breaking criteria changes in a linear trend once breaking events occur

$$\eta_t^*=\begin{cases}\eta_t^F, & t \geq T^* \\ \eta_t^I+\dfrac{t-t_0}{T^*}(\eta_t^F-\eta_t^I), & 0 \leq t-t_0 < T^*\end{cases} \quad (7)$$

$T$* is the transition time with the default value $5(h/g)^{1/2}$, $t_0$ is the time where breaking occurs, and $t$ is the duration of wave breaking. $\eta_t^I=(0.65-0.35)\sqrt{gh}$ and $\eta_t^F=0.15\sqrt{gh}$ are the critical values for wave breaking initiation and cease. Though default values have been proposed (see [14][15]), the previous research also shows that they also vary within a large range depending on the specific forms of the governing equations.

In addition to the energy dissipation due to wave breaking, subgrid-scale turbulent processes associated with surf zone eddies may become an important factor influencing the flow pattern of the wave-generated current field(Chen et al., [16]; Nwogu [21]). The turbulence that occurs in regions with large gradients in the horizontal velocities is therefore simulated by the Smagorinsky type subgrid model [16][17][21], introduced in the momentum equations, to account for the effect of the resultant eddy viscosity on the underlying flow. The subgrid mixing term($\boldsymbol{R}_s$) has the same form as Eq.(5), but the eddy viscosity due to the subgrid turbulence has the form of

$$\upsilon_s = C_m\Delta x\Delta y[(U_x)^2+(V_y)^2+(U_y+V_x)^2/2]^{1/2} \quad (8)$$

in which $U$ and $V$ are the velocity components of the time-averaged underlying current field(in the present study they are estimated every two wave period), $\Delta x$ and $\Delta y$ are the grid spacing in the $x$(cross shore) and $y$ (longshore) directions respectively, and $C_m$ is the mixing coefficient whose values have been assumed ranging between 0.1 and 2.0.

The bottom shear stress is given by a quadratic term written in the form of:

$$\boldsymbol{R}_f = -C_f(h+\eta)^{-1}\boldsymbol{u}\left|\boldsymbol{u}\right| \quad (9)$$

where $C_f$ is the friction coefficient with default value range 0.001-0.01. It should be noted that $\boldsymbol{R}_f$ is inversely proportional to local water depth. So this term is important for wave transformation in shallow water and hence contributes favorable to the nearshore circulation patterns.

## 2.3 Numerical Scheme and Boundary Conditions

The equations are solved numerically by using a finite-difference method on rectangular grid system. Higher order finite difference formula is used to approximate both spatial and temporal derivatives in the equations. While time integration is made by using the 3rd order Adams-Bashforth predictor and a 4th order Adams-Moulton corrector. This numerical scheme is extensively used for solving Boussinesq models and the details are referred to [15]. The theoretical analysis of the stability conditions for this algorithm is provided in [22]. By applying the Von Neumann stability analysis to the present Boussinesq model, the similar expressions can be obtained. For the predictor algorithm, it is stable when the Courant number is smaller than or equal to unity, and for the corrector algorithm, the Courant number is smaller than or equal to 0.5. In the following numerical simulations, the time step and space step satisfy this stable condition.

At the offshore boundary, the relaxation zone method for generating non-reflective waves (Bingham and Agnon [23]) is used. Our numerical experiments show that this method is more effective to generate high nonlinear and large period waves than the internal wave generation method embodied in FUNWAVE2D, which may be due to the fact that the internal source function is derived using linearized Boussinesq equations. As slot method is used, the rest three boundaries are treated as closed solid walls, and sponger layer is placed at the shoreward end of the domain to absorb any outgoing wave energy. However for longshore current simulations, periodic lateral cross-shore boundaries are imposed, following the suggestion from Chen et al. [16]and Chen and Svendsen [24].

The entire computational domain is treated as an active fluid domain by using permeable sea-bed technique, where the beach is considered porous or containing narrow slots, thus the moving shoreline is considered, the details of this method is referred to [14] or [16].

# 3 Numerical Results and Discussions

Except specially addressed elsewhere, a Cartesian coordinate system is adopted with origin located on the still water plane (SWL) with $x$ axis increases offshore ward, $y$ axis directs longshore direction and $z$ axis pointing vertically upwards. And all the time-averaged quantities are obtained after the steady state of wave field are reached.

## 3.1 Normally Incident Solitary Wave Shoaling Over Plane Beaches

To illustrate the necessity of incorporating fully nonlinear terms in the Boussinesq equations, the shoaling of solitary waves over plane beaches is simulated. This example is a good benchmark test as the wave height to water depth ratio reached prior to breaking is extremely high and thus nonlinearity is strong. In addition, solitary waves propagate as an isolated pulse without extra background disturbances and thus allowing clearly examining the model performances. Two different slopes of 1:35 and 1:100 are used in the computations and the numerical results from weakly nonlinear model and fully nonlinear model are plotted in Figure 1. Where the numerical solution from FNPF model(Fully Nonlinear Potential Flow, Wei et al. [13]) is also presented as the analytical solutions to the problem.

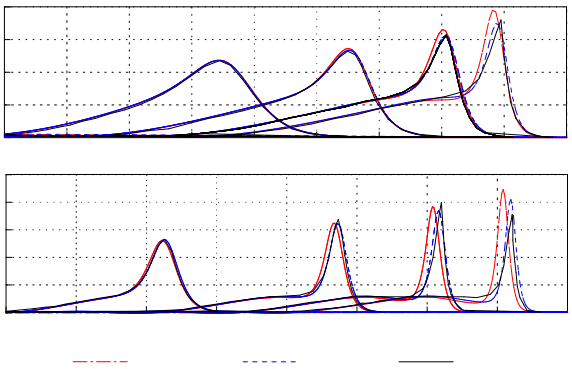

Fig.1 Wave profiles of shoaling solitary waves over plane beaches. In the figure the length/height, time variables are scaled by $h_0$ and $(h_0/g)^{1/2}$, respectively. While $H_0$ and $h_0$ are solitary wave height and water depth over flat bottom respectively. $x$'=0 is defined at beach toe and $x$' increases shoreward while $t$=0 is defined at the time when solitary wave crest reaches beach toe.

It could be seen from the figure that in the relatively deep water, the weakly nonlinear and fully nonlinear models have almost the same performance as the nonlinearity is not so strong. However as the nonlinearity increases under the effect of shoaling, the differences between two models become apparent. The weakly nonlinear model fails to predict both wave amplitude and wave phase, while the fully nonlinear model presents much better results. The discrepancy between two models is amplified when the beach slope becomes mild as the shoaling effect is strengthened thereby.

## 3.2 Normally Incident Regular Waves Breaking Over Plane Beaches

1D periodic waves breaking over plane beaches will be considered. First the experimental data for breaking cnoidal waves from Ting and Kirby [25] is used to investigate the role of each of the breaking parameters. To avoid other effects on the numerical results, bottom friction and moving shoreline boundary are not considered.

The numerical experiments show that the numerical results are not sensitive to $\eta_t^F$ and thus default value 0.15 $(gh)^{1/2}$ is used. The value of $\eta_t^I$ could be easily determined by matching the breaking point to the measurement, which is found to be $0.80(gh)^{1/2}$. Three values of breaking strength $C_{br}$=0.6, 1.2, 1.8 are used for simulation and the computed results are plotted in Figure 2(a). Where as expected, small breaking strength fails to effectively dissipate wave height after wave breaking. While the values of 1.2 and 1.8 primarily show the same results, hence the default value 1.2 is used in this paper. Keep $C_{br}$=1.2, three simulations are done using $T^*$=(2.5,5.0,7.5) $(h/g)^{1/2}$ and the numerical results are given in Figure 2(b). Three values primarily present the similar results except slight difference near the breaking point. Hence we also use the recommended value $T^*=5.0(h/g)^{1/2}$ for 1D breaking waves.

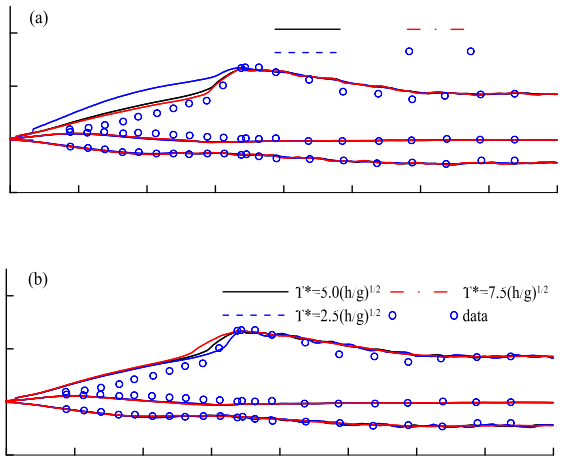


Fig.2 The effect of breaking strength coefficient $C_{br}$(a) and breaking duration parameter $T^*$ (b) on the numerical results.

| Cases | $h_0$(m) | H(m) | L(m) | T(s) | Breaking type | Δx(m) | Δt(s) |
|---|---|---|---|---|---|---|---|
| A10112 | 0.36 | 0.067 | 1.44 | 1.00 | Spilling | 0.02 | 0.01 |
| 061071 | 0.36 | 0.067 | 2.87 | 1.67 | Spilling | 0.02 | 0.01 |
| 031041 | 0.36 | 0.043 | 3.53 | 2.00 | Plunging | 0.02 | 0.01 |
| 041041 | 0.36 | 0.039 | 4.52 | 2.50 | Spilling-plunging | 0.02 | 0.01 |
| 051041 | 0.36 | 0.036 | 6.12 | 3.33 | Spilling | 0.02 | 0.01 |

Table 1: Wave conditions and simulation parameters for 1D regular waves breaking over plane beaches. ($h_0$ is the water depth over flat bottom, H, L and T are the incident wave height, wave length and wave period, respectively.)

Another five tests for regular waves breaking over plane beaches [26], covering a wide range of breaker types, are considered for validation. Wave characteristics for all waves tested and the simulation parameters are listed in Table 1.

The computed results including wave height and mean water level are presented in Figure 3. In the figure the increase of wave height during shoaling process and the initiation of wave breaking, the subsequent decrease of wave height are well reproduced and the setup trend are also predicted well. While for all the tests (including those in Figure 2), the wave heights in the inner surf zone tend to be over-predicted by the model in the case of breaking point are captured. This phenomenon are also found by other researchers, [14][27]for example, when they carried out Boussinesq-type simulation. The discrepancy, in our opinion, is caused by the intrinsic limitation of using the eddy viscosity mechanism to approximately mimic wave breaking in the model. Considering the empirical treatment of wave breaking, the agreements between the numerical results and measurements are reasonably good.

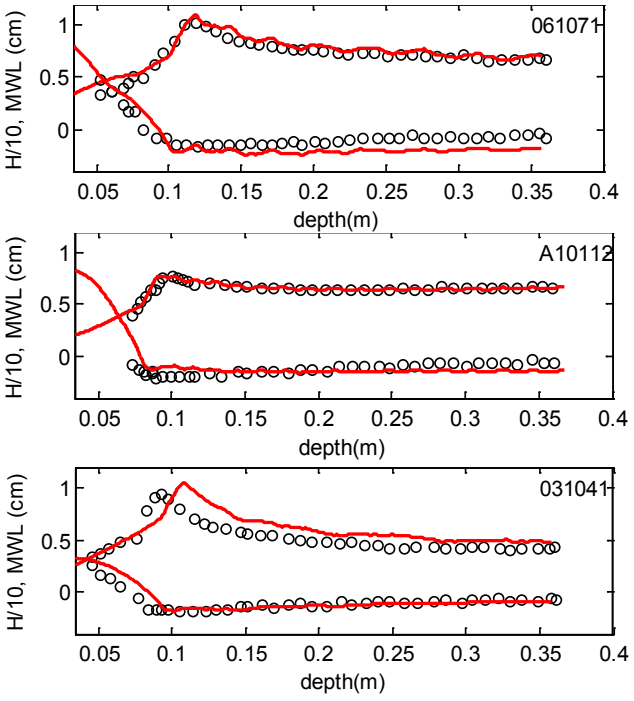


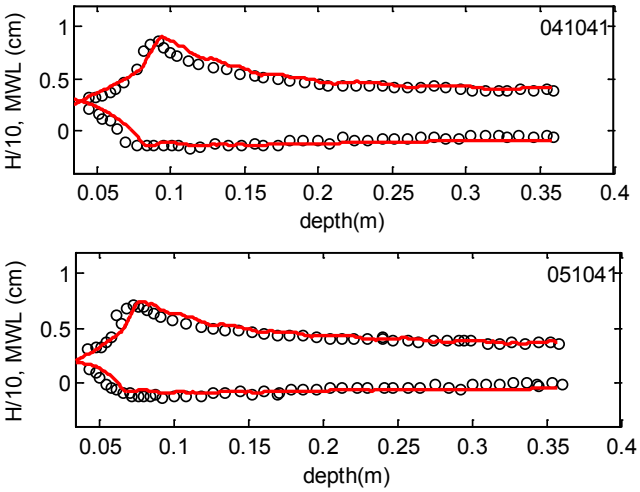


Fig.3 The comparison of wave height and mean water level between numerical results(solid line) and experiment data(symbols) for five cases of regular waves breaking over plane beach.

### 3.3 Obliquely Incident Waves Breaking on Plane Beaches

Visser [28] has conducted experiments to investigate the obliquely incident waves breaking on plane beach, in the experiments free surface elevation and wave-induced longshore currents are detailed collected and they will be used here for model validation.

A snapshot of the 3D computed free surface elevation and phase-averaged current field for case 4 (see Table 2) of Visser experiments [28] are presented in Figure 4(a) and Figure 4(b) respectively. It is seen from this figure that the modelled wave crest becomes narrow and asymmetric while wave trough becomes flat during shoaling process. The increase and decrease of wave height before and after breaking event are well reproduced. The longshore currents are quite steady and uniform alongshore, indicating the proper and efficiency of the numerical implementation, especially the treat of periodic lateral cross-shore boundary condition, relaxation zone method for wave generation, and this will definitely increase the confidence of obtaining reliable results using the model.

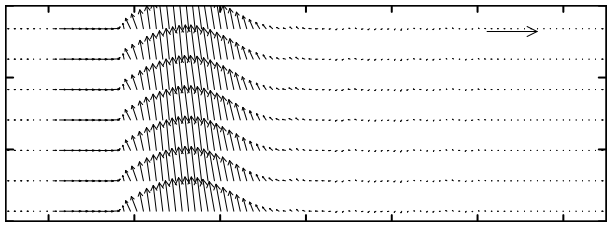

Fig.4 The instantaneous surface elevation(a) and the mean current filed(b) for case 4 of Visser's experiment.

Also using case 4, numerical experiments are conducted to investigate the parameter values effect on the computed results and the corresponding results are plotted in Figure 5.

First there values of bottom friction coefficient $C_f$=0.003, 0.006 and 0.01 are used. Clearly, wave height and mean water level are not very sensitive to this parameter while the amplitude of longshore currents is greatly controlled by this parameter. The increase of $C_f$ results in apparently the decrease of the longshore current amplitude. Numerical experiments also show that neglecting bottom friction($C_f$ =0) causes computation blow up while the extremely large value of $C_f$ (=0.01) deteriorates the computed wave heath near the breaking point. Then $C_f$=0.006 is kept constant and there values of breaking strength $C_{br}$=0.6, 1.2 and 1.8 are used for simulation and the computed results are also presented in Figure 5. Clearly, small value fails to effectively decrease the wave height in surf zone and to correctly predict the location of the longshore currents crest. While the large value only provides marginal improvements of wave height in surf zone and tends to cause longshore currents biased offshore. Then we keep $C_f$=0.006, $C_{br}$=1.2 and there values of subgrid mixing $C_m$=0.05, 1.0 and 2.0 are used for simulation. As seen in the figure, large value results in oscillations of surface elevations while mean water level and longshore currents are not very sensitive to this parameter. Large variation of $C_m$, even over one order of magnitude is observed to result in a few percent changes. This is in consistent with the conclusions drawn by Mendonca et al. [29]. Chen et al. [16] also found the amplitude of dissipation caused by subgrid turbulence is smaller compared against those by breaking, though the former spreads seaward away the breaking point while the latter is strongly localized in surf zone. In this paper, $C_m$=1.0 is used.

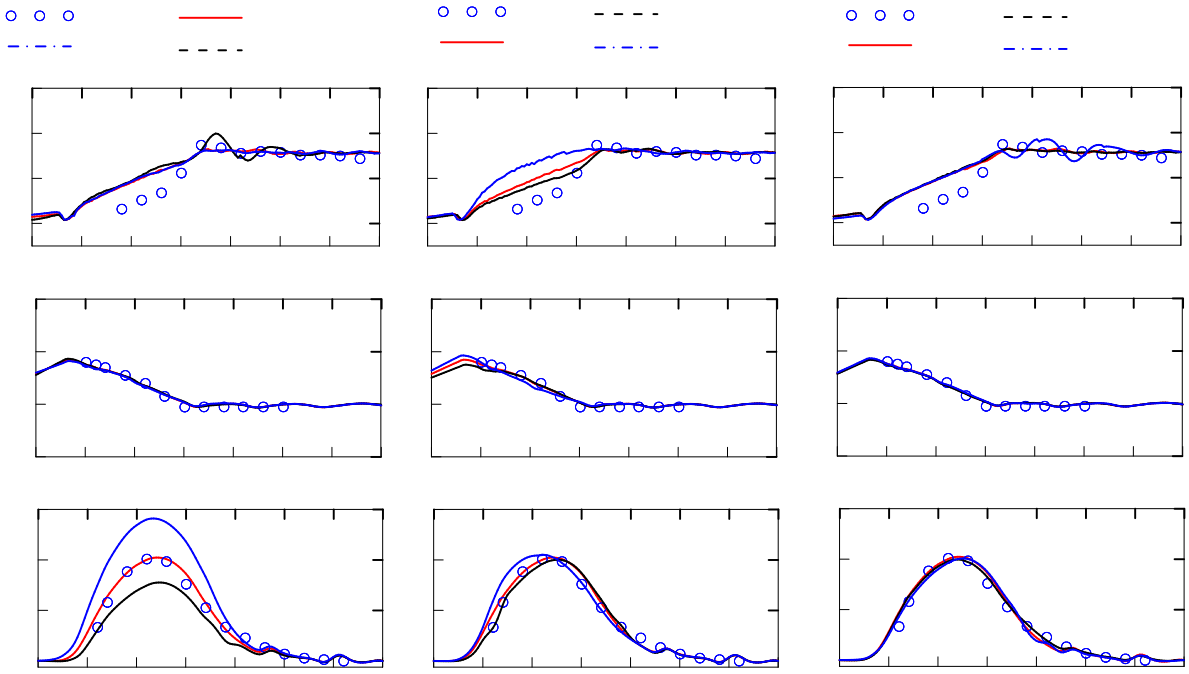

Fig.5 The effect of bottom friction(left), breaking strength(middle) and subgrid mixing(right) on the computed wave height(a), mean water level(b) and mean current profile(c).

| Cases | Beach slope | H(cm) | $h_0$(cm) | T(s) | $\alpha$ | Breaker type | $\Delta$x (cm) | $\Delta$y (cm) | $\Delta$t (s) |
|---|---|---|---|---|---|---|---|---|---|
| 2 | 0.101 | 9.5 | 39.9 | 1.00 | 30.5 | Plunging | 5.0 | 7.24 | 0.02 |
| 4 | 0.050 | 7.8 | 35.0 | 1.02 | 15.4 | Plunging | 5.0 | 9.24 | 0.02 |
| 5 | 0.050 | 7.1 | 34.8 | 1.85 | 15.4 | Plunging | 7.5 | 13.3 | 0.02 |

Table 2: Experiment cases of Visser [27] and simulation parameters (where $h_0$ is the water depth over flat bottom, H and T are the incident wave height and wave period, respectively. $\alpha$ is the angle of incidence wave.)

Via the above process, the tunable parameters are determined as $C_{br}$=1.2, $C_f$=0.006, $C_m$=1.0. To test the applicable range of these parameters, the rest two cases(case 2 and case 5) of Visser experiments (see Table 2) are simulated and the numerical results are compared against the experimental data in Figure 6. Generally the numerical results and experimental results are in good agreements. Wave height increases due to nonlinear shoaling and decrease after breaking are well predicted. The variation trend of the mean water level is also captured by the model. The wave height however in the inner surf zone is also overestimated, just as found in section 3.2 for 1D breaking waves. The distribution of longshore currents profile, including the magnitude and the location of the crest value are generally in good agreements with the experimental data. It is also noteworthy to mention that three cases considered here belong to plunging breaker while the eddy viscosity method is originally designed for spilling breaker with mild energy dissipation.

The computed mean current field are shown in Figure 7. For two cases considered, the computed results show high longshore uniformity of longshore currents. Comparing the results for cases 2, 4 and 5, the effect of different incident waves on the final mean current field also could be observed.

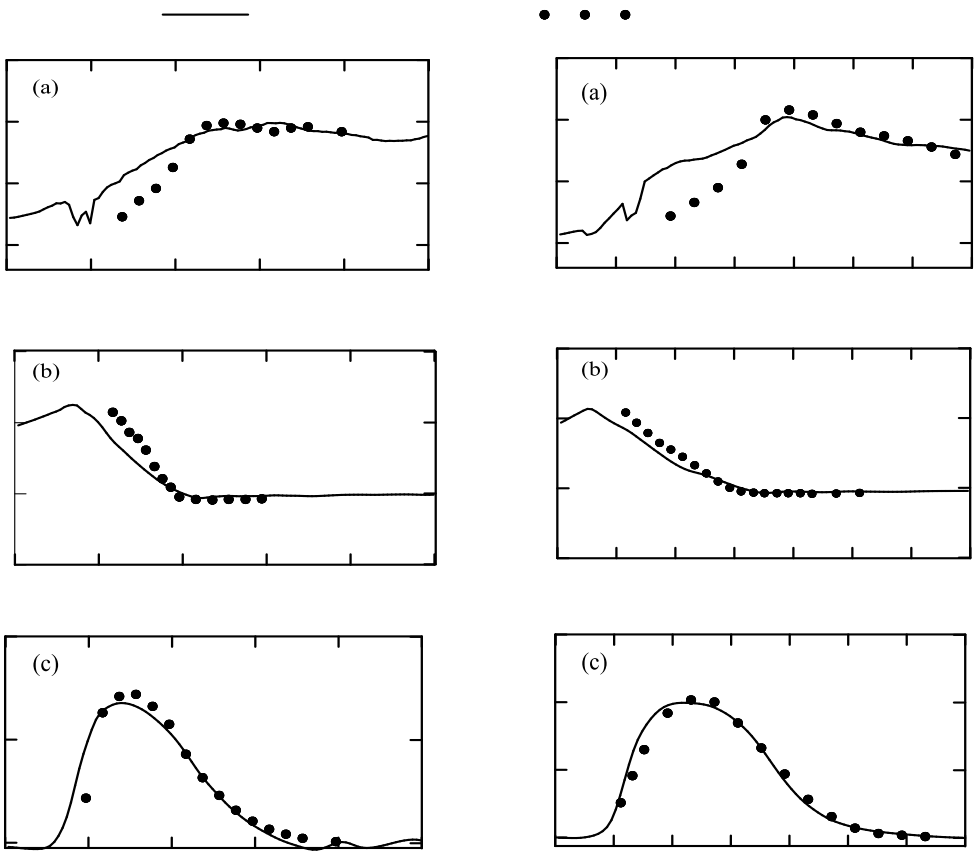


Fig.6 The comparison of wave height(a), mean water level(b) and longshore current profile(c) between computed results and experimental data for case 2(left) and case 5(right) of Visser's experiments.

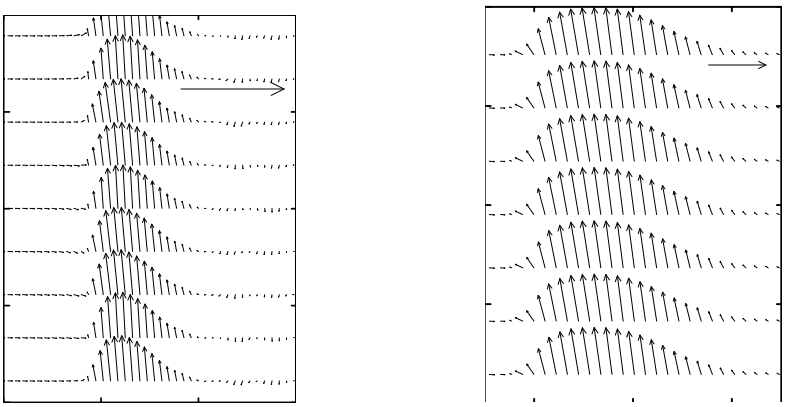

Fig.7 The mean current field for Case 2(left) and Case 5(right) of Visser's experiments.

### 3.4 Normal Incident Waves Breaking on Barred Beaches

The experimental data of breaking waves on a barred beach, collected by Haller et al. [30], are widely used for model validation[18][21]. In the experiments, a longshore uniform bar, incised by two rip channels, is superposed on a plane beach to mimic the typical feature of a real barred beach. The spatial variation of the wave-induced excess momentum flux will finally drive a time-varying circulation pattern—rip current system. The experiment is believed to reproduce the main features of the bathymetry-controlled rip current in real nature.

Neglecting the small variations from longshore uniformity in the planar beach and considering slight asymmetry about the center axis of the physical wave basin, the idealized top half of the bathymetry is used for simulation, see Figure 8 for the details. Numerical simulations were carried out for test B which corresponds to a normally incident regular wave with period, $T$=1s and height, $H$=0.048m on a constant water depth 0.363m. The grid-space and time-step increments are $\Delta x$=0.05m, $\Delta y$=0.10m and $\Delta t$=0.01s. Simulation duration is 300s and the computed datasets from last 200s are used for statistical analysis.

The computed wave height and mean water level(MWL) along three cross-shore transects are plotted in Figures 9 and 10, respectively. The experimental data and the numerical results from FUNWAVE2D are also presented. The agreements between the present model and measurements are good. Wave breaking point, wave height decrease after wave breaking and the corresponding variation of MWL(setdown and setup) are well captured by the model. Especially the delayed wave breaking in rip channel due to relatively deep water in the channel, wave height increase in the offshore ward of the rip channel due to the interaction of propagation waves and offshore directed current are simulated. The wave height is greatly over-predicted by present model and FUNWAVE2D in the offshore region of rip channel(y=4.6m), which is due to the delayed instability motion of rip current on an ideal bathymetry, as also explained in Chen et al. [18]. Except the slight accurate result of setup in inner surf zone, the present model and FUNWAVE2D primarily have the same performance.

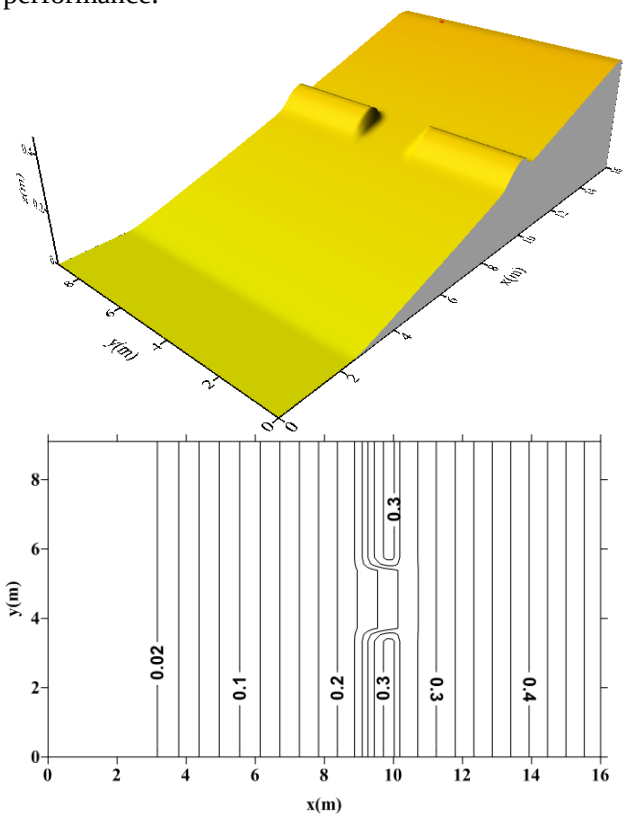


Fig.8 The 3D(top) and contour(bottom) map of barred beach with rip channel (with the origin defined at the lower left corner).

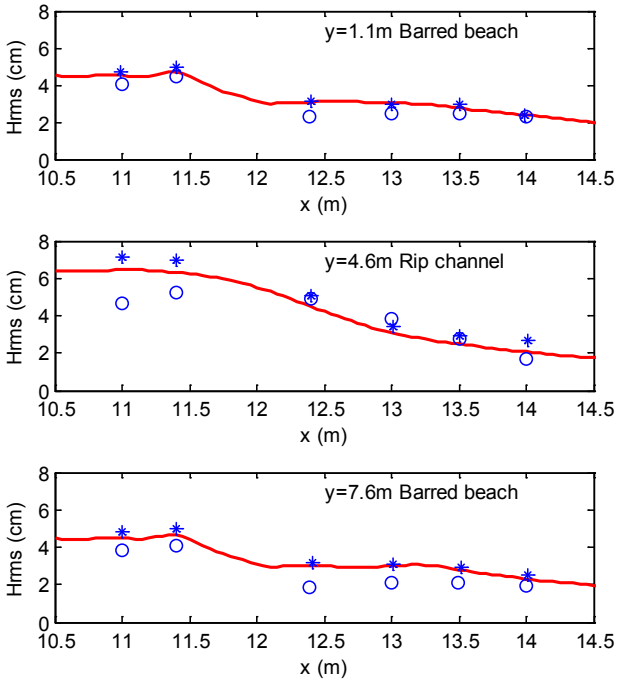


Fig.9 The comparisons of wave height between numerical results from present model(solid line), from FUNWAVE2D(stars) and measurements(circles).

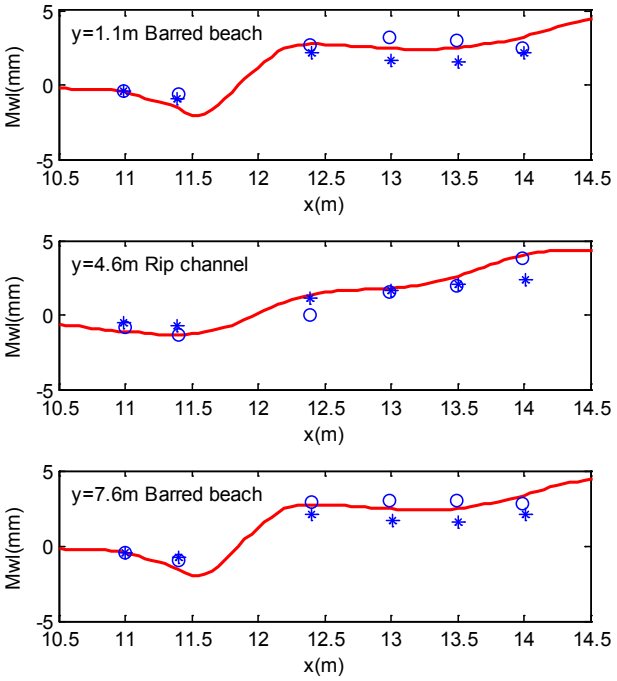


Fig.10 The comparisons of mean water level between numerical results from present model(solid line), from FUNWAVE2D(stars) and measurements(circles).

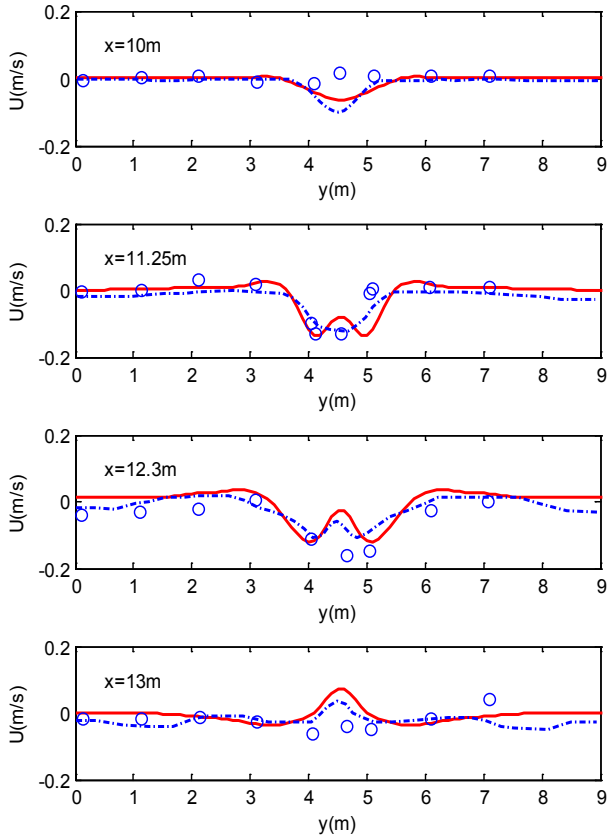


Fig.11 The comparisons of cross-shore mean current (U) between numerical results from present model (solid line), from FUNWAVE2D(dash-dotted line) and measurements(circles).

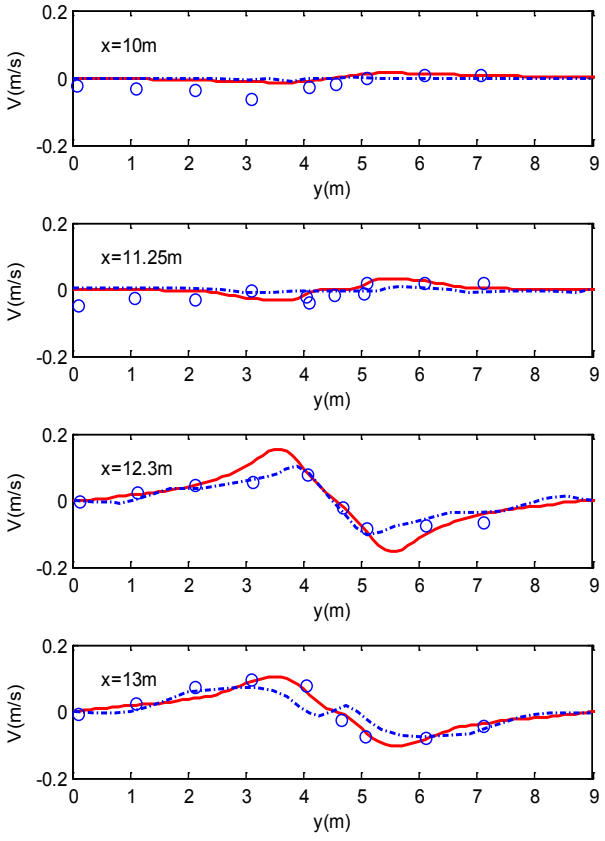


Fig.12 The comparisons of longshore mean current (V) between numerical results from present model (solid line), from FUNWAVE2D(dash-dotted line) and measurements(circles)

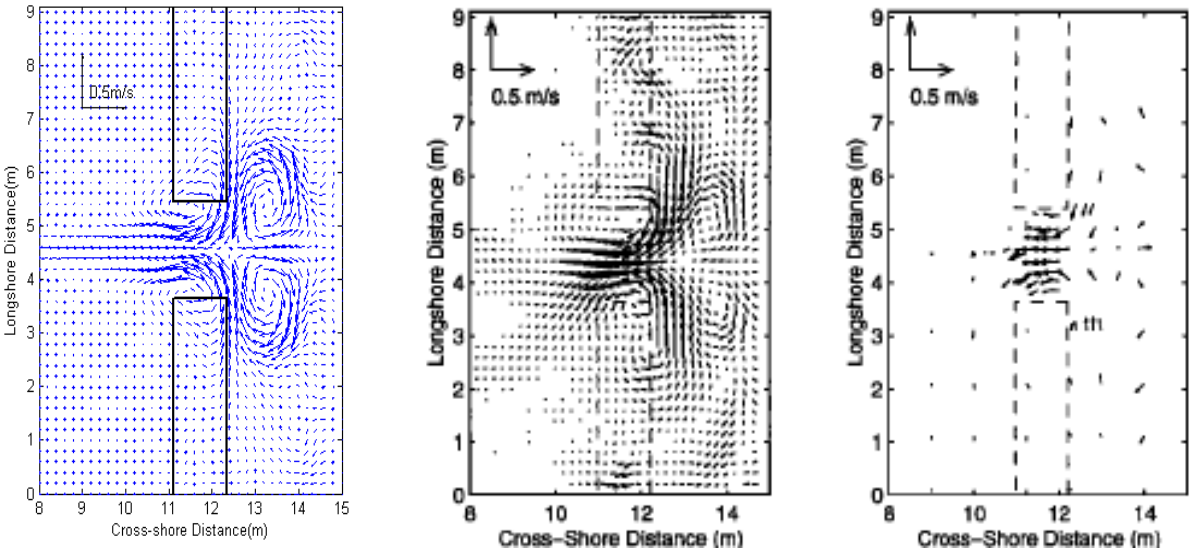


Fig.13 The comparisons of mean current field from present model(left), from FUNWAVE2D(middle) and experiments(right).

The longshore mean current($U$) and the cross-shore mean current($V$) are compared against the experimental data and the numerical results from FUNWAVE2D in Figures 11 and Figure 12, respectively. Generally the simulated mean current components agree well with the measurements. First, the variation trend of the offshore directed mean current (rip current) is well captured. The over-prediction of U nearshore shoreline ($x$=13m) and the under-estimation of $U$ in rip channel ($x$=11.25m and $x$=12.3m) are observed for the present model and FUNWAVE2D, which may be due to the use of ideal bathymetry instead of experimental bathymetry, as also argued by Chen et al. [18]. Secondly, the variation of longshore current, which have the opposite sign and consist of rip feeder, are also predicted well by the model.

The computed mean current field is shown in Figure 13 and compared against the measurements and the numerical result from FUNWAVE2D. The flow field predicted by the numerical model is similar to the measured velocity field. The main components of a rip current system, namely, rip current, rip feeder and rip neck are reproduced by the model. Two numerical models also predict a shoreward mean flow and secondary circulation close to the shoreline, which however is not apparent in measurements due to the sparse measurements. The measured rip current shows bias toward the bottom, while the numerical results from the present model and FUNWAVE2D show much symmetry about the center axis and the computed rip current penetrate farther to deep water. This is also attributed to the use of ideal bathymetry (with strict symmetry) instead of experimental bathymetry (with slight asymmetry), as the instability motion of rip current is delayed on the ideal bathymetry [18].

More insight into the generation and motion of rip current could be obtained by examining the time-dependent variation of computed quantities, such as free surface elevation, mean current filed and vorticity field (defined as $V_x$-$U_y$ and estimated every two wave period in simulation). The numerical results at four moments, i.e., $t$=20s, 80s, 120s and 180s, are shown in Figure 14. At the initial stage $t$=20s, the computed wave crests are primarily parallel to the shore with the wave height in the rip channel is higher than that on the bar profiles, which is due to the fact that the depth-induced breaking is delayed in rip channel. Meanwhile the vortex rings are seen to be generated on the seaward bar-channel intersects. And the offshore directed mean current also could be observed between clockwise and anti-clockwise rotation vortex. With the subsequent waves breaking on the bathymetry ($t$=80s, 120s, 180s), the vortex rings are released into deep water and the strength of rip current grows gradually. The process of generation and release of vortex rings is repeated subsequently. Additionally a secondary circulation pattern close to the shoreline is also found to feed the rip current. The increase of the wave height at the region where the rip current and incident waves coexist are apparent, denoting the applicability of Boussinesq-type model in describing the interaction between waves and currents.

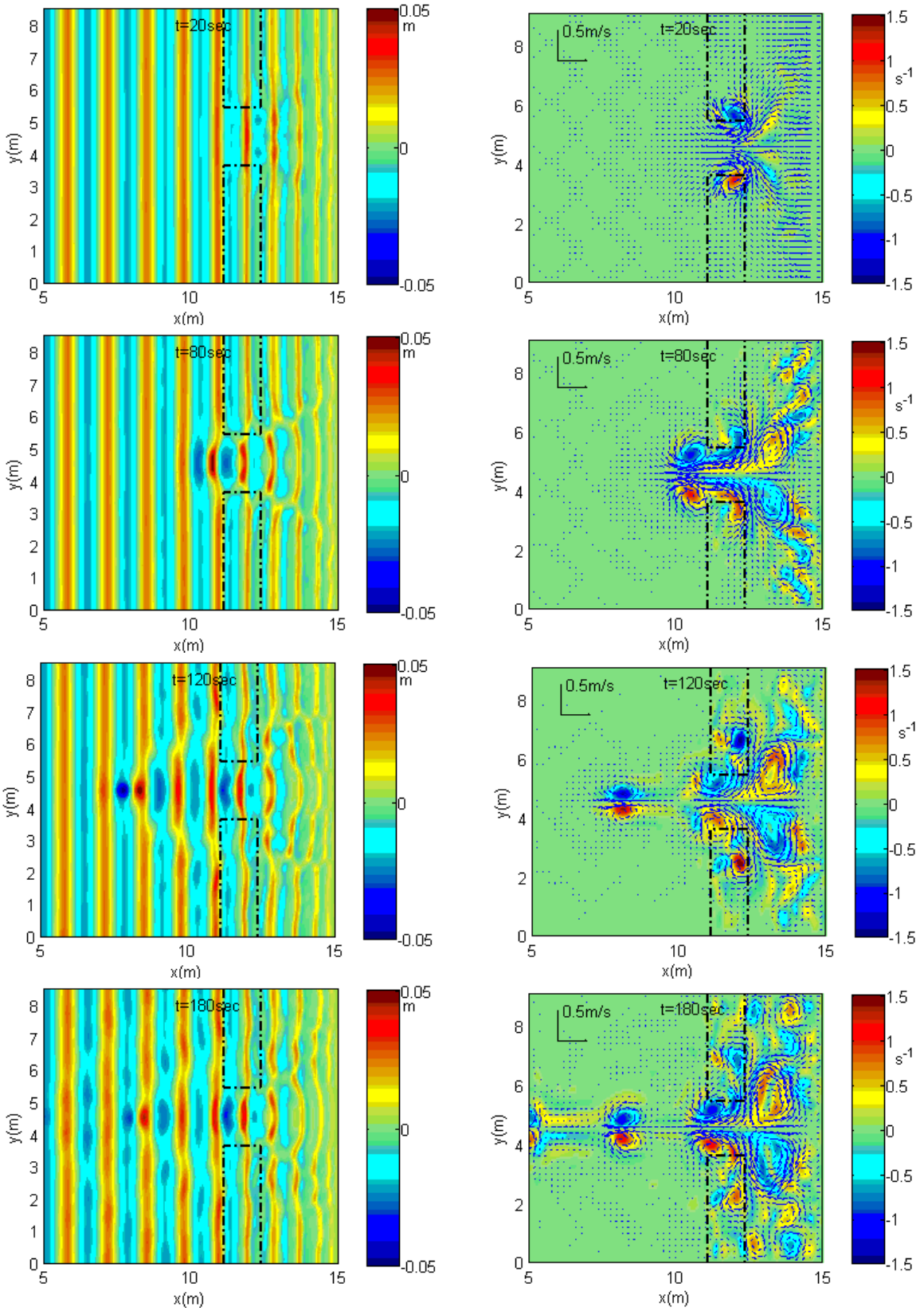


Fig.14 The instantaneous free surface elevation(left) and vector field, vortex(right) at four moments.

## 4 Conclusions

A numerical model, based on the fully nonlinear Boussinesq equations, is developed to simulate the nonlinear wave breaking waves and wave-induced longshore currents with the main conclusions are drawn below.

(1) The numerical results of shoaling of solitary waves demonstrate the necessity of incorporating

fully nonlinear characteristics in the equations. The model has shown itself to accurately predict nonlinear wave transformation in the surf zone. Breaking phenomena and associated mean currents are predicted both qualitatively and quantitatively for a variety of 1D and 2D tests over complex bathymetries.

(2) For waves breaking over plane beaches, the model is observed to over-predict wave heights in the inner surf zone, which is in consistent with other researchers. It suggests that proper method to deal with wave breaking in a Boussinesq-type model still needs further investigation.

(3) Parameter analyses are conducted for waves breaking on plane beaches. For normally incident waves, the numerical results are found less sensitive to breaking related parameters(except for initiation parameter) and the variation only result in marginal difference near wave breaking point and thus recommended default values are adopted. For oblique incident waves, we found that the mean water level is not sensitive to the variation of parameters, while the profiles of mean longshore current greatly depend on the breaking strength and bottom friction, while subgrid mixing has a negligible effect.

(4) The main features of a rip current system could be qualitatively and quantitatively reproduced by the model. The discrepancy between the numerical model and measurements are mainly attributed to the use of ideal bathymetry instead of experimental bathymetry.

As the first step of developing a fully nonlinear model and validation aim, only time-averaged quantities are considered in the present paper. Bearing in mind that, however, Boussinesq-type wave models belong to phase-resolving type and they describe intra-wave properties. Though not pursued in present study, further investigation on intra-wave properties, coupled wave-wave, wave-current interaction and also their contribution to the pollutant/sediment transport are still in process.

## 5 Acknowledgments

The authors gratefully acknowledge the financial support from the National Natural Science Foundation of China Grant no. (51009018), Key Laboratory of Water-Sediment Sciences and Water Disaster prevention of Hunan Province (Grant No. 2013SS02 and 2012SS02).

*References:*

[1]. Boussinesq J., Theorie des ondes et des remous qui se propagent le long d'un canal rectangulaire horizontal, en communiquant au liquide contenu dans ce canal des vitesses sensiblement pareilles de la surface au fond, *J. Math. Pures Appl.*, Series.2, no.17, 1872, pp.55-108.

[2]. Korteweg D.J. and G. de Vries, On the change of form of long waves advancing in a rectangular canal and on a new type of long stationary wave, *Phil. Mag.*, Series5, no.39, 1895, pp.422-443.

[3]. Peregrine D.H., Long waves on a beach, *J. Fluid Mech.*, vol.27, no.4, 1967, pp.813-827.

[4]. Kirby J.T., Boussinesq models and applications to nearshore wave propagation, surf zone processes and wave-induced currents, *in Advances in Coastal Modeling, Oceanogr. Ser.*, V.C. Lakhan, Ed., Elsevier, New York, 2003, pp.1-41.

[5]. Madsen P.A., Murray R. and Sørensen O.R., A new form of Boussinesq equations with improved linear dispersion characteristics, *Coastal Engineering*, vol.15, no.4, 1991, pp.371-388.

[6]. Madsen P.A. and Sørensen O.R., A new form of the Boussinesq equations with improved linear dispersion characteristics, Part 2. A slowly-varying bathymetry, *Coastal Engineering*, vol.18, no.3-4, 1992, pp.183-204.

[7]. Nwogu O., An alternative form of the Boussinesq equations for nearshore wave Propagation, *Journal of Waterway, Port, Coastal, and Ocean Engineering*, vol. 119, no.6, 1993, pp. 618–638.

[8]. Madsen P.A. and Schäffer H.A., Higher order Boussinesq-type equations for surface gravity waves—derivation and analysis, *Phil. Trans. R Soc Lond A*, vol.356, no.1794, 1998, pp.3123–3186.

[9]. Madsen P.A., Bingham H.B. and Schäffer H.A., Boussinesq-type formulations for fully nonlinear and extremely dispersive water waves: derivation and analysis, *Phil. Trans. R Soc Lond A*, vol.459, no.2033, 2003, pp.1075–1104.

[10]. Gobbi M.F., Kirby J.T. and Wei G., A fully nonlinear Boussinesq model for surface waves. Part 2. Extension to $O(kh)^4$, *Journal of Fluid Mechanics*, vol.405, no.4, 2000, pp.181–210.

[11]. Zou Z. and Fang K., Alternative forms of the higher-order Boussinesq equations: Derivations and validations, *Coastal Engineering*, vol.55, no.6, 2008, pp.506-521.

[12]. Zou Z., A new form of higher order Boussinesq equations, *Ocean engineering*, vol.27, no.5, 2000, pp.557-575.

[13]. Wei G., Kirby J.T., Grilli S.T. and Subramanya R., A fully nonlinear Boussinesq model for surface waves: Part I. Highly nonlinear

unsteady waves, *Journal of Fluid Mechanics*, vol.294, 1995, pp.71–92.
[14]. Kennedy A.B., Chen Q., Kirby J.T. and Dalrymple R.A., Boussinesq modeling of wave transformation, breaking, and runup. Part I: 1D, *Journal of Waterway, Port, Coastal, and Ocean Engineering*, vol.126, no.1, 2000, pp.39–47.
[15]. KIRBY J. T., WEI G., *et al*. FUNWAVE 1.0 Fully nonlinear Boussinesq wave model documentation and user's manual, *Research Report No. CACR-98-06*, Center for applied Coastal Research, University of Delaware, Newark, 1998.
[16]. Chen Q., Kirby J.T., DalrympleR.A. , Kennedy A.B., Chawla and Arun, Boussinesq Modeling of Wave Transformation, Breaking, and Runup. II: 2D, *Journal of Waterway, Port, Coastal, and Ocean Engineering*, vol.126, no.1, 2000, pp.48-56.
[17]. Chen Q., Kirby J. T., Dalrymple R. A., Shi F. and Thornton E. B., Boussinesq modeling of longshore currents, *Journal of Geophysical Research*, vol.108, no. c11, 2003, pp.1-26.
[18]. Chen Q., Boussinesq modeling of a rip current system, *Journal of Geophysical Research*, vol.104, no.c9, 1999, pp.20617-20637.
[19]. Mil-Homens J., Fortes C. J.E.M. and Pires-Silva A. A., An evaluation of wave propagation simulations over a barred beach with a Boussinesq-type model, *Ocean Engineering*, vol.37, no.1, 2010, pp.236-251.
[20]. Zou Z., Higher order Boussinesq equations, *Ocean Engineering*, vol.26, no.8, 1999, pp.767-792.
[21]. Nwogu O.K., Numerical prediction of rip current on barred beaches, *Proceedings of the 4th International Symposium on Ocean Wave Measurement and Analysis*, San Francisco, USA, 2001, pp.1396-1405.
[22]. Lin, P. and C. Man. A staggered-grid numerical algorithm for the extended Boussinesq equations. *Applied Mathematical Modelling*, vol. 31, no.2, 2007, pp. 349-368
[23]. Bingham H.B. and Agnon Y., A Fourier-Boussinesq method for nonlinear water waves, *Eur. J. Mech. B/Fluids*, vol.24, no.2, 2005, pp.255-274.
[24]. Chen Q. and Svendsen I.A., Effects of cross-shore boundary condition errors in nearshore circulation modeling, *Coastal Engineering*, vol.48, no.4, 2003, pp.243-256.
[25]. Ting F. C. K., and Kirby J. T., Dynamics of surf-zone turbulence in a spilling breaker, *Coastal Eng.*, vol.27, no.3-4, 1996, pp.131–160.
[26]. Hansen J. B. and Svendsen I. A., Regular waves in shoaling water: Experimental data, *Tech. Rep. ISVA Ser.*, 21, Technical Univ. of Denmark, Denmark, 1979.
[27]. Zaleski A.R., A numerical model for breaking waves in the surf zone, Dissertation, Technical University of Denmark, 2007.
[28]. Visser P. J., Laboratory measurements of uniform longshore current, *Coastal Engineering*, vol.15, no.5-6, 1991,pp.563-593.
[29]. Mendonca A., Brocchini M., Besio G.., Piattella A., Flow mixing solutions of a Boussinesq-type model: towards a dispersive HLES, *Proc. 7th Asian Computational Fluid Dynamics Conference*, Bangalore, India. 2007, pp. 189.
[30]. Haller M.C., Dalrymple R.A. and Svendsen I.A. Experiments on Rip current dynamics and nearhsore circulation, *Research Report No. CACR-00-04*, Center for applied Coastal Research, University of Delaware, Newark, 2000.